Nanocomposite electrical generator based on piezoelectric zinc oxide nanowires

K. Momeni, G. M. Odegard, and R. S. Yassar[a)]
Department of Mechanical Engineering-Engineering Mechanics, Michigan Technological University, 1400 Twonsend dr, Houghton, Michigan 4993, USA

(Received 13 September 2010; accepted 18 October 2010; published online 1 December 2010)

A nanocomposite electrical generator composed of an array of zinc oxide nanowires is considered. The electric potential distribution along zinc oxide nanowires is modeled using continuum mechanics and Maxwell's equations for the case of axial loading. A perturbation technique is used for decoupling the constitutive equations. The governing differential equations are solved using a finite difference method. It is shown that a gradient of electric potential exists along the axis of the zinc oxide nanowires. Maximum and minimum values of electric potential exist at the extreme ends along the nanowire length and have opposite signs. The positive and negative voltages are separated by a zero-valued electric potential at the middle of the nanowire. It is also shown that the electric potential is a strong function of shear stress at the interface of matrix-nanowire. The proposed system and loading configuration can generate up to 160% more electric potential than the values reported for the nanowire in the bended configuration, which results in a more sustainable energy source. © *2010 American Institute of Physics*. [doi:10.1063/1.3517095]

I. INTRODUCTION

Energy generation utilizing piezoelectric materials has been well-studied over the past two decades.[1–5] In particular, ZnO nanowires (NWs) (Refs. [1,2]) have potential application for nanodevices[2–4] because of their piezoelectric response, large aspect ratio,[5] superior mechanical properties relative to bulk zinc oxide,[6–8] and low production costs. There are some reports on the generation of electric potential by bending ZnO NWs,[4,9,10] however, using piezoelectric nanomaterials for energy harvesting applications is still a matter of debate.[4,11] Multiscale modeling can facilitate the development of nanodevices that incorporate ZnO NWs by predicting the overall piezoelectric response as a function of structural geometry.

Piezoelectricity of nanomaterials has been a subject of current research in the scientific community. There are reports on enhancement of piezoelectricity in nanomaterials compared to bulk materials.[4] Using finite element method simulations followed by an experimental setup, it has been shown that electrical voltage can be generated due to mechanical bending of ZnO NWs.[4,12] Presence of Schottky diode between the nanomaterial and Atomic Force Microscopy (AFM) tip used for deflecting the nanomaterial plays the main role in voltage generation.[10,13,14]

Many modeling studies have been performed on similar piezoelectric materials. Piezoelectricity of one-dimensional (1D) nanostructures has been modeled using first-principle calculations,[15–17] molecular dynamics simulations,[18–20] and continuum models.[12,21,22] Piezoelectric composites reinforced with piezoelectric fibers used for energy harvesting have also been the topic of theoretical[23–25] studies. It has been proven that piezoelectric-fiber composites have a higher output voltage-to-applied load ratio than bulk piezoelectric ceramic materials owing to the large length-to-area ratio of the reinforcing fibers.[26] During the finalization of this paper, it was found out that a nanocomposite electrical generator was built experimentally.[27] The reported experimental results were also showing a gradient of electric potential along the axis of the ZnO NWs which is in agreement with the model derived in this work.

The objective of this study is to develop a multiphysics analytical model that predicts the electric potential generated by a *nanocomposite electrical generator* composed of ZnO NWs embedded in a finite epoxy matrix, as shown in Fig. 1. Modeling the electric potential generated by the nanocomposite electrical generators would be a major step toward the design of self-powered Micro/Nano Electro Mechanical Systems (MEMS/NEMS) devices. As a first step, an analytical model is developed in the form of a nonhomogenous second order partial differential equation which predicts the stress

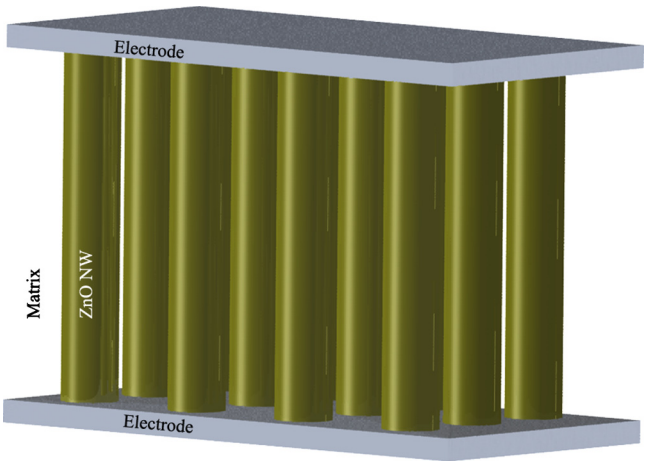

FIG. 1. (Color online) Schematic picture of naonocomposite electrical generator made up of piezoelectric ZnO NWs embedded in epoxy matrix.

[a)]Electronic mail: reza@mtu.edu.

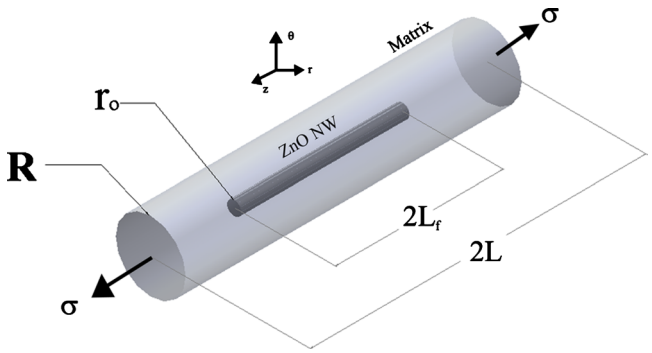

FIG. 2. (Color online) RVE of a ZnO NW with length of $2L_f$ embedded in a matrix with length of $2L$. The composite is subjected to the overall stress of σ along the cylindrical axis. R is the outer radius of the RVE and r_o is the radius of the ZnO NW.

and electric potential field distributions in an individual ZnO NW embedded in a finite epoxy matrix. A numerical method was utilized to solve the analytical model which is singular along the axis of the NW. This information is subsequently used in a larger-scale multiphysics model of the nanocomposite electrical generator. The predicted distribution of electric potential along the ZnO NWs in the nanocomposite electrical generator demonstrates that it is capable of generating an electric potential that is more than twice as much as that produced from bended stand-alone ZnO NWs.

II. MODELING OF ZNO NWS IN AN EPOXY MATRIX

The first step in the multiscale modeling procedure was to predict the piezoelectric response of a single ZnO NW embedded in an epoxy matrix. The representative volume element (RVE) is shown in Fig. 2. The ZnO NW and the epoxy matrix were both modeled as elastic isotropic materials. Although modeling ZnO NW as an isotropic material might not be the best choice, it simplifies the calculations while keeping the results in an acceptable approximation.[12] The bonding between the ZnO NW and epoxy matrix was assumed to be perfect. Simple longitudinal tensile loading along the axis of the NW was modeled, which is the direction in which NWs have the maximum reinforcing effect. The ZnO NW was modeled as a perfect cylinder.

The general mechanical and electrical field equations, i.e., conservation of linear momentum and Gauss's law of electric field, were used in combination with constitutive equations to derive the analytical relation between the applied load and potential distribution along the NW. The shear-lag model was used to describe the load transfer between the matrix and NW.[28] This model has been successfully used for modeling 1D nanostructures.[29,30]

The conservation of linear momentum in the absence of body forces and acceleration is:

$$\nabla \cdot \mathbf{T} = \mathbf{0}, \tag{1}$$

where $\mathbf{T}$ is the stress tensor. Gauss's law in the absence of free charges is:

$$\nabla \cdot \mathbf{D} = \mathbf{0}, \tag{2}$$

where $\mathbf{D}$ is the electric displacement vector. The mechanical and electrical responses of the ZnO NW, assuming linear piezoelectric behavior, are coupled via the constitutive equations as follows:[31]

$$\mathbf{T} = \mathbf{c}_E\mathbf{S} - \mathbf{e}^T\mathbf{E}, \tag{3a}$$

$$\mathbf{D} = \mathbf{e}\mathbf{S} + \boldsymbol{\kappa}\mathbf{E}, \tag{3b}$$

where $\mathbf{S}$ is strain tensor, $\mathbf{E}$ is the electric field vector, $\mathbf{c}_E$ is the elastic stiffness tensor, $\mathbf{e}$ is the piezoelectric constant tensor, $\boldsymbol{\kappa}$ is permittivity tensor, and $\mathbf{e}^T$ is the transpose of the tensor $\mathbf{e}$. The electric field vector is related to the electric potential field ϕ via:

$$\mathbf{E} = -\nabla\phi. \tag{4}$$

The constitutive equations [Eq. (3)] are coupled via the piezoelectric constant tensor. Using perturbation theory,[12] the perturbation parameter λ is introduced in the piezoelectric constants by defining a virtual material such that $\mathbf{e}' = \lambda\mathbf{e}$. The mechanical and electrical properties of the virtual material are assumed to be equal to those of the real material. For $\lambda = 1$ the virtual material behaves the same as the real material, while for $\lambda = 0$ there is no coupling of the mechanical and electrical properties between the two materials. For $0 < \lambda < 1$, the mechanical and electrical properties of the virtual material are coupled to the real material to a limited degree. The mechanical and electrical response of the material can be expressed in terms of the order of perturbation correction, l, using infinite power series:

$$\begin{cases} T_p(\lambda) = \lim\limits_{l\to\infty} \sum\limits_{n=0}^{l} \lambda^n T_p^{(n)} \\ S_q(\lambda) = \lim\limits_{l\to\infty} \sum\limits_{n=0}^{l} \lambda^n S_q^{(n)} \\ E_k(\lambda) = \lim\limits_{l\to\infty} \sum\limits_{n=0}^{l} \lambda^n E_k^{(n)} \\ D_i(\lambda) = \lim\limits_{l\to\infty} \sum\limits_{n=0}^{l} \lambda^n D_i^{(n)} \end{cases}, \tag{5}$$

where superscript n represents the approximation order of the variable. For the zeroth-order approximation the constitutive equations are:

$$\mathbf{T}^{(0)} = \mathbf{c}_E\mathbf{S}^{(0)}, \tag{6a}$$

$$\mathbf{D}^{(0)} = \boldsymbol{\kappa}\mathbf{E}^{(0)}. \tag{6b}$$

The electrical and mechanical properties of the virtual material are decoupled for the zeroth-order approximation. For the first-order approximation the constitutive equations become:

$$\mathbf{T}^{(1)} = \mathbf{c}_E\mathbf{S}^{(1)} - \mathbf{e}^T\mathbf{E}^{(0)}, \tag{7a}$$

$$\mathbf{D}^{(1)} = \mathbf{eS}^{(0)} + \boldsymbol{\kappa}\mathbf{E}^{(1)}. \tag{7b}$$

Assuming zero initial electric field, i.e., $\mathbf{E}^{(0)}=0$, equation set (7) becomes:

$$\mathbf{T}^{(1)} = \mathbf{c}_E\mathbf{S}^{(1)}, \tag{8a}$$

$$\mathbf{D}^{(1)} = \mathbf{eS}^{(0)} + \boldsymbol{\kappa}\mathbf{E}^{(1)}. \tag{8b}$$

Equation (8) shows that the mechanical response of the virtual material as a first-order approximation is independent of its electrical properties while the electrical response depends on its zeroth-approximation mechanical response. It can be shown that for higher-orders of approximation the mechanical and electrical responses of the virtual material are coupled.[12] Therefore, using higher-order approximations may give more accurate results, however, they will not be helpful for simplifying the solution. Assuming the electric response of the material does not affect its mechanical deformation, the first order approximation is sufficient for the calculations that are described below.

The geometry and loading configuration of this problem is axisymmetric. Therefore, the three-dimensional (3D) problem reduces to a two-dimensional problem in terms of z and r (Fig. 2). Using the shear-lag model, assuming the radial strain of NW to be much less than its axial strain (i.e., $\varepsilon_{rr} \ll \varepsilon_{zz}$ for the NW) and $R \gg r_o$ (low concentration of NWs), the stress along the ZnO NW in terms of the cylindrical coordinate system is:[30]

$$T_{zz} = \sigma[(1-A)\mathrm{ch}(\alpha z)/\mathrm{ch}(\alpha L_f) + A], \tag{9a}$$

$$T_{rz} = \sigma r/2[\alpha(A-1)\mathrm{sh}(\alpha z)/\mathrm{ch}(\alpha L_f)], \tag{9b}$$

$$T_{rr} = \nu_f(T_{zz} + T_{rz}), \tag{9c}$$

where σ is the applied axial stress and ν_f is the ZnO Poisson's ratio. The A and α parameters are defined as follows:

$$A = R^2/[r_o^2 + E_m/E_f(R^2 - r_o^2)], \tag{10}$$

$$\alpha = \sqrt{\frac{R^2 - r_o^2}{r_o^2(1+\nu_m)}} \times \frac{r_o^2 + (R^2 - r_o^2)E_m/E_f}{R^4 \ln(R/r_o) - 1/4(R^2 - r_o^2)(3R^2 - r_o^2)}, \tag{11}$$

where ν_m is the Poisson's ratio for the matrix material and E_m and E_f represent the Young's modulus of the matrix and NW, respectively.

The following dimensionless variables are defined:

$$\phi^* = \phi\frac{(E_f/\sigma)}{r_o e_{33}/\kappa_{11}}, \tag{12}$$

$$r^* = r/r_o, \tag{13}$$

$$z^* = z\alpha, \tag{14}$$

$$H = \alpha r_o. \tag{15}$$

After substituting Eqs. (6a) and (8b) into Eq. (2) and using Eq. (4), the governing differential equation for electric potential along the NW is

$$\frac{\partial^2\phi^*}{\partial r^{*2}} + \frac{1}{r^*}\frac{\partial\phi^*}{\partial r^*} + H^2\frac{\kappa_{33}}{\kappa_{11}}\frac{\partial^2\phi^*}{\partial z^{*2}} = \left\{\frac{1}{2}\left[\nu_f^2 r^* + (\nu_f^2 - \nu_f)r^*\frac{e_{31}}{e_{33}}\right]\cosh(z^*)H^2 + \left[1 - \nu_f^2 - (\nu_f^2 + \nu_f)\frac{e_{31}}{e_{33}} - (\nu_f + 1)\frac{e_{15}}{e_{33}}\right]\sinh(z^*)H\right\}B, \tag{16}$$

where B is defined as follows:

$$B = \frac{1}{\cosh(\alpha L_f)}\left(1 - \frac{R^2}{r_o^2 + \frac{E_m}{E_f}(R^2 - r_o^2)}\right). \tag{17}$$

Equation (16) is a second-order nonhomogeneous partial differential equation with variable coefficients. This type of equation can only be solved using numerical methods. An appropriate numerical method must be chosen that can accurately handle the singularity in Eq. (16) at the NW axis. In Sec. IV the numerical approach that is used to overcome the singularity point is discussed.

III. NUMERICAL METHOD

Equation (16) must be solved to get the electric potential distribution along the NW. It was assumed that the surface potential at the boundary of the NW and the potential gradient, $\partial\phi/\partial z$, at the extreme ends of the NW were both zero. Equation (16) is in terms of two independent variables: radius r, and longitudinal axis z. Therefore, it is possible to use two different numerical solution methods for solving the problem along each of r and z coordinates. Finite Fourier transformation was used along the z-axis and the finite difference method was used along the r-axis.

Considering the Neumann boundary conditions along the z-axis, the cosine Fourier transform for the dimensionless potential function along the z-axis, Φ^*, was

$$\Phi_k^*(r) = \sum_{j=0}^{N_Z-1}\phi_j(r,z_j)\cos\left(\frac{\pi k(j+1/2)}{N_Z}\right), \tag{18}$$

where N_Z is the number of points along the z-axis and z_j is defined as

$$z_j = \left(j + \frac{1}{2}\right)\Delta_z, \quad j = 0,1,\ldots,N_Z - 1, \tag{19}$$

where $\Delta_z = 2L_f/N_Z$. Using the Fourier transform that was defined in Eq. (18), the dimensionless differential Eq. (16) becomes:

$$\frac{\partial^2\Phi_k^*}{\partial r^{*2}} + \frac{1}{r^*}\frac{\partial\Phi_k^*}{\partial r^*} - H^2\frac{\kappa_{33}}{\kappa_{11}}\frac{1}{\Delta_z^2}\left(\frac{\pi k}{N_z}\right)^2\frac{\partial^2\Phi_k^*}{\partial z^{*2}} = \mathrm{P}_k, \tag{20}$$

where P_k is the transformed form of the right hand side of Eq. (16) using the cosine Fourier transform that was used for ϕ. After some mathematical manipulation, Eq. (20), in its finite difference form everywhere except on the axis (i.e., $j \geq 1$), is:

$$\Phi^*_{k,j-1}\left(1-\frac{1}{2j}\right)+\Phi^*_{k,j+1}\left(1+\frac{1}{2j}\right)-\Phi^*_{k,j}\left[2+H^2\frac{\kappa_{33}}{\kappa_{11}}\frac{\Delta_r^2}{\Delta_z^2}\left(\frac{\pi k}{N_Z}\right)^2\right]=\Delta_r^2 P_{k,j}, \tag{21}$$

where $\Delta_r = r_o/N_R$ and r are discretized as

$$r = j\Delta_r, \quad j = 0,1,\ldots,N_R. \tag{22}$$

The second term in Eq. (20) is singular at $r=0$. Using L'Hopital's rule and $\partial\Phi^*/\partial r=0$ at $r=0$, the finite differential form of Eq. (20) for the axis of NW is

$$4\Phi^*_{k,1}-\left[4+H^2\frac{\kappa_{33}}{\kappa_{11}}\frac{\Delta_r^2}{\Delta_z^2}\left(\frac{\pi k}{N_z}\right)^2\right]\Phi^*_{k,0}=\Delta_r^2 P_{k,0}. \tag{23}$$

Defining γ_j, β_j, ξ_k, and $S_{k,j}$ as follows:

$$\gamma_j = 1-\frac{1}{2j}, \tag{24a}$$

$$\beta_j = 1+\frac{1}{2j}, \tag{24b}$$

$$\xi_k = -\left[2+H^2\frac{\kappa_{33}}{\kappa_{11}}\frac{\Delta_r^2}{\Delta_z^2}\left(\frac{\pi k}{N_z}\right)^2\right], \tag{24c}$$

$$S_{k,j} = \Delta_r^2 P_{k,j} \tag{24d}$$

The set of Eqs. (20) and (23) can be written as

$$\begin{bmatrix} \xi_k-2 & 4 & 0 & \cdots & & & \\ \gamma_1 & \xi_k & \beta_1 & \cdots & & & \\ & & & \cdots & & & \\ & & & \cdots & \gamma_{N_R-2} & \xi_k & \beta_{N_R-2} \\ & & & \cdots & 0 & \gamma_{N_R-1} & \xi_k \end{bmatrix} \cdot \begin{bmatrix} \Phi_{k,0} \\ \Phi_{k,1} \\ \vdots \\ \Phi_{k,N_R-2} \\ \Phi_{k,N_R-1} \end{bmatrix} = \begin{bmatrix} S_{k,0} \\ S_{k,1} \\ \vdots \\ S_{k,N_R-2} \\ S_{k,N_R-1}-\beta_{N_R-1}\Phi_{k,N_R} \end{bmatrix}. \tag{25}$$

Solving Eq. (25) for $\Phi_{k,i}$, $(i=0,\ldots,N_R-1)$ provides the electric potential along the diameter of the NW at node k on the z-axis in the frequency domain. Using the inverse Fourier transform, the values in real space for electric potential along z-axis at each node is given by:

$$\phi_{j,i} = \frac{1}{N_z}\Phi_{0,i}+\sum_{k=1}^{N_z-1}\Phi_{k,i}\cos\left(\frac{\pi k(j+1/2)}{N_z}\right), \tag{26}$$

where $\phi_{j,i}$ is the electric potential of jth node on z-axis and ith node on r-axis. Equation (26) is the closed-form solution of the electric potential distribution at each node of the NW.

IV. CASE STUDY

Equation (16) was solved using the above-described numerical method. The epoxy matrix was assumed to have the following properties: $E_m=2.41$ GPa and $\nu_m=0.35$.[32] To fulfill the assumption of low NW concentration, it was assumed that $R=5\ r_o$. The dimensions of the ZnO NW were assumed to be the same as those reported in the literature,[12] i.e., $r_o=25$ nm; $2L_f=600$ nm.

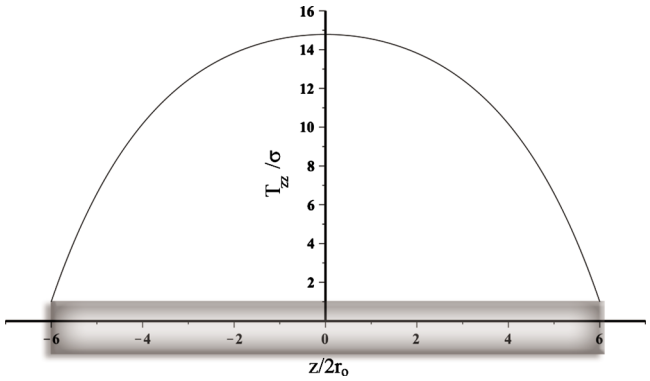

FIG. 3. (Color online) The dimensionless axial stress distribution T_{zz}/σ along the axis of NW $z/2r_o$, for a ZnO NW of $r_o=25$ nm and $2L_f=600$ nm is plotted. The schematic of the NW is shown as a solid gray cylindrical overlaid on the $z/2r_o$ axis. The loading configuration dictates the load to transfer to the NW through the matrix material. At the extreme ends the stress that transfers to the end caps is the same magnitude as the applied stress, σ. Moving away from the NW ends, axial stresses increase due to an increase in transferred shear stresses between the matrix and NW, with the maximum at $z=0$.

The reported Young's modulus of ZnO NWs is widely scattered. The elastic modulus values have been measured to be 52 GPa with the dual-mode resonance method,[33] 58 GPa with mechanical resonance experiments,[34] 31 GPa with three-point bending tests,[35] 40 GPa in cantilever bending,[36] 97 GPa with tensile tests,[37] and 29 GPa in a single-clamped NW bending experiment.[38] Also, a number of theoretical studies have demonstrated a relationship between the diameter of the ZnO NWs and their mechanical properties. Density functional theory[10] and taking into account the surface stress effect which is defined as the reversible work required to stretch a surface elastically[39] are among those theoretical models. In the current study the elastic modulus of the NW was assumed to be $E_f=129$ GPa.[40]

From Eq. (9a) the dimensionless mean axial stress, T_{zz}/σ, is plotted versus dimensionless position along the axis of the NW, i.e., $z/2r_o$, in Fig. 3. Using Eq. (9b), the dimensionless shear stress, T_{rz}/σ, between the ZnO NW/matrix interface is plotted along the axis of the NW, $z/2r_o$, in Fig. 4.

The permittivity of the bulk ZnO is $\kappa_{11}=7.77\kappa_0$, $\kappa_{22}=\kappa_{11}$, and $\kappa_{33}=8.91\kappa_0$, where κ_0 is the permittivity of a vacuum $\kappa_0=8.854\times10^{-12}$ A s/V m.[41] The piezoelectric constants are $e_{31}=-0.51$ C/m^2, $e_{33}=1.22$ C/m^2, and $e_{15}=-0.45$ C/m^2 which has been measured for ZnO films.[42] Using these values and Eq. (26), the distribution of electric potential along the NW was determined and is plotted in Fig. 5. The figure shows the dimensionless electric potential, ϕ^*, at different radii except on the surface of the NWs, which is assumed to have no electric potential. In Fig. 5 the z^*-axis is shifted to the left compared to Figs. 3 and 4 to enhance the visualization of the results. Therefore the origin of the coordinate system is placed at the left end of NW. It also should be noted that $z^*=z\alpha$. It can be seen that the extremums of

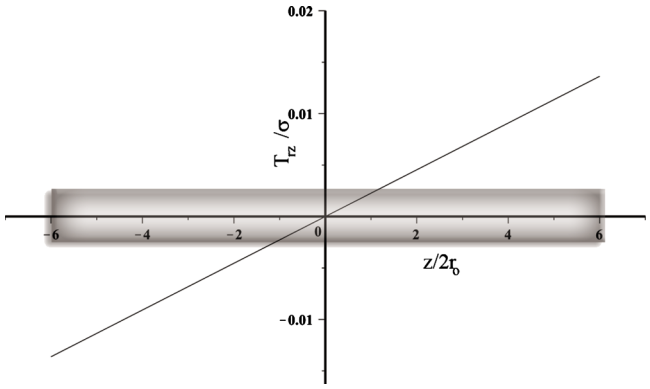

FIG. 4. (Color online) Dimensionless shear stress distribution T_{rz}/σ along the axis of NW $z/2r_o$, for a ZnO NW of r_o=25 nm and $2L_f$=600 nm. The schematic of the NW is shown as a solid gray cylindrical overlaid on the $z/2r_o$ axis. The maximum shear stress occurs at extreme ends of the NW; i.e., $\tau=\tau_{max}$ at $z=\pm L_f$, while it vanishes at the middle of the NW, $T_{rz}/\sigma=0$ at $z=0$.

electric potential are at the extreme ends ($z^*\approx 10$ and $z^*=0$) of the NW along the z^*-axis. The electric potential vanishes at the center of the NW, i.e., $z^*=0$.

It can be seen that the generated electric potential is a strong function of the shear stress, i.e., it is extremum at the ends and zero at the middle of the NW. Also the slopes of the curves are zero at the extreme ends of the NW, which is consistent with the governing Neumann boundary conditions.

Considering the definition of ϕ^* [Eq. (12)], the generated electric potential, ϕ, is directly proportional to the applied stress, σ. Therefore, to find the maximum generated electric potential in a nanocomposite electrical generator, the strength of the nanocomposite material needs to be known. Generally, in polymer matrix composites with a ceramic reinforcement phase, the interface bonding between the polymer and reinforcement phase is relatively weak compared to the rest of the material system. In order to use the maximum shear stress theory[43] the shear strength of ZnO NW/epoxy matrix interface needs to be known. Since there does not appear to be any data available for the shear strength of the ZnO NW-epoxy interphase in the literature, the shear

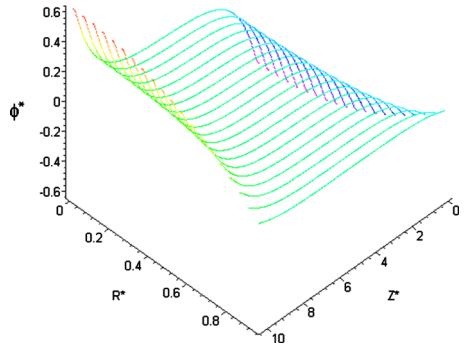

FIG. 5. (Color online) Electric potential distribution along the z-axis for a ZnO NW of r_o=25 nm and $2L_f$=600 nm is shown. The electric potential is extremum at the extreme ends of the NW with opposite signs. The NW behaves as a generator with a positive charge at one end and a negative charge at the other end while the charges are separated by zero voltage at the middle of the NW. The difference between the maximum and minimum values of the dimensionless electric potential is $\Delta\phi^*\approx 1.2$.

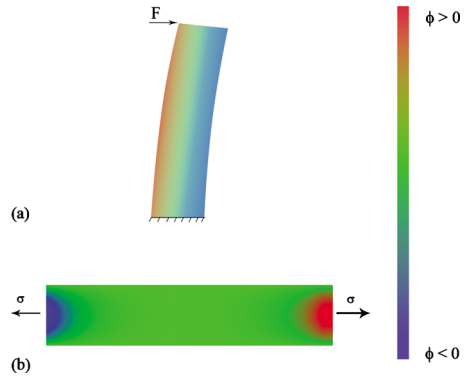

FIG. 6. (Color online) Schematic of the electric potential distribution (a) along a ZnO NW and (b) along a NW embedded in an epoxy matrix. While the generated electric potential for a ZnO NW is along its diameter, the generated electric potential for a ZnO NW in a nanocomposite electrical generator is along its axis.

strength of the interface of glass fiber/epoxy was used instead as a close approximation. The maximum value of the shear stress on the ZnO NW, which is shown in Fig. 4, is $T_{rz}^{max}=0.015\sigma$. Assuming $T_{rz}^{max}=3$ MPa,[44] the maximum applied stress is $\sigma_{max}=200$ MPa.

From Fig. 5, the difference between the extremum values of dimensionless electric potential is $\Delta\phi^*=1.2$. Considering the maximum applied stress $\sigma_{max}=200$ MPa, and using the definition of ϕ^* [Eq. (12)], the maximum generated electric potential is more than 0.8 V. This is ~260% of the value reported for the bended ZnO NWs (Ref. 12) (~0.3 V). Therefore a single ZnO NW embedded in an epoxy matrix is capable of producing higher electric voltage compared to the values reported for bended ZnO NWs.

A key issue in any piezoelectric generator is the sustainability of the electric potential, i.e., the time constant of the corresponding RC circuit. The time constant of the corresponding RC circuit for a material is directly related to the magnitude of electric field and number of free carriers inside the material. A higher electric field results in a larger force on free carriers within the material. A larger applied force increases free carrier mobility, which reduces the time constant. This issue was first discussed by Alexe *et al.*[11] and is expected to decrease the magnitude of electric potential generation in a bended ZnO NW by canceling the displacive charges.[4]

A distribution of the electric potential in ZnO NW determines the magnitude of the electric field in the material which consequently specifies the sustainability of the electric potential. A schematic picture of electric potential distribution along a ZnO NW in a bended configuration is shown in Fig. 6(a), using the analytical formulation reported in the literature.[12] The electric potential gradient is along the diameter of the ZnO NW which is on the order of tens of nanometers. The electric potential distribution is also shown along a ZnO NW embedded in an epoxy matrix in Fig. 6(b), using the method proposed here.

For a the ZnO NWs embedded in epoxy matrix the separation of charges are in the order of tens of micrometers. A simple parallel plate capacitor model was used, to get a rough estimate of the electric field which is formed inside the NW:

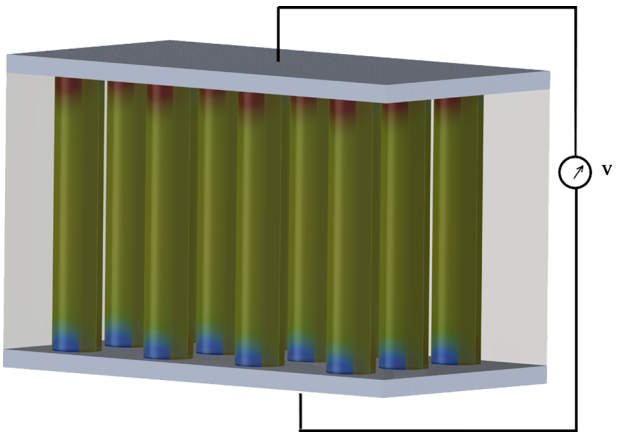

FIG. 7. (Color online) 3D schematic picture of the proposed nanocomposite generator system made of ZnO NWs embedded in an epoxy matrix is shown. While one end of the NWs has a positive electric potential, the other end has a negative electric potential.

$$E = \frac{V}{d}, \tag{27}$$

where E is the electric field, V is the electric potential between the two plates, and d is the separation distance of the two plates. While for a NW subjected to bending the separation distance, d, is on the order of a few tens of nanometers, for a ZnO NW embedded in matrix subjected to axial stress, it is in the order of a few tens of microns. Therefore the electric field in the NW and consequently the driving force on free carriers inside the NW is much smaller for the individual elements of a nanocomposite electrical generator (shown in Fig. 1) compared to the bended NW. Smaller driving force lowers the charge mobility which consequently increases the generated voltage stability. Furthermore, the free carriers have to travel a longer distance in the case of a nanocomposite electrical generator compared to a nanogenerator, in order to cancel the displacive charge generated due to the piezoelectric effect. It can be concluded that a nanocomposite electrical generator is a more sustainable energy source compared to a NW subjected to bending.

A schematic picture of a nanocomposite electrical generator with electric potential distribution along the ZnO NWs is shown in Fig. 7 which was depicted based on the results shown in Fig. 6(b). In this configuration, the ZnO NWs act as a series of voltage sources connected in parallel.

The voltage that can be produced by a nanocomposite electrical generator is equal to the voltage produced by the individual ZnO NWs. However, the power capacity of the generator is proportional to the number of its constituent NWs. These relations can be summarized as

$$V_{\mathrm{NCEG}} = V_{\mathrm{NW}}, \tag{28a}$$

$$I_{\mathrm{NCEG}} = \sum_{n} I^{n}_{\mathrm{NW}}, \tag{28b}$$

where V_{NCEG} and I_{NCEG} are voltage and current of nanocomposite electrical generator. V_{NW}, I_{NW}, and n are voltage, current, and index of each constituent ZnO NW. The efficiency of our nanocomposite electrical generator scan be quantified by calculating the electric energy stored in the NW divided by the work that was done by the external force on the RVE. This will be studied in our future work.

V. CONCLUSION

A new configuration has been introduced for a nanostructured energy generator which consists of an array of ZnO NWs embedded in an epoxy martial, which is subjected to tensile loading. The analytical model for predicting the generated electric potential was developed. The governing differential equation of the electric potential distribution of constituent ZnO NWs was a singular nonhomogeneous elliptical differential equation with variable coefficients. This differential equation was solved numerically. Dimensions and properties of a ZnO NW that were previously reported in the literature were assumed.

The predicted electric potential gradient was aligned along the axis of the NW. That is, positive and negative potentials were located at the ends of the NW and separated by a zero-valued electric potential at the middle. This electrical potential gradient leads to lower electric fields inside the NW in the nanocomposite electrical generator compared to the field generated by ZnO NW subjected to bending. Therefore, the nanocomposite electrical generator is a more sustainable energy source relative to typical nanogenerators using bent ZnO NWs.

The distribution of axial and shear stresses along the ZnO NW was also calculated. While axial stress was maximized in the middle of the NW, the shear stress was maximized at the ends of the NW. Also, the distribution of electric potential was attributed to shear stress transfer at the interface of NW and the surrounding polymer matrix.

There are reports on the effect of electromechanical boundary conditions on elasticity of zinc oxide NWs.[45] However, such effect has not been studied in this paper. Including effect of electromechanical boundary conditions on elasticity of embedded ZnO NWs will be investigated as an expansion to this model.

ACKNOWLEDGMENTS

We appreciate Dr. A. Soghrati and NSF-CMMI Grant No. 0926819 for providing the financial support.

[1] J. Zhou, P. Fei, Y. Gao, Y. Gu, J. Liu, G. Bao, and Z. L. Wang, Nano Lett. **8**, 2725 (2008).
[2] P. X. Gao, J. Song, J. Liu, and Z. L. Wang, Adv. Mater. **19**, 67 (2007).
[3] J. Song, J. Zhou, and Z. L. Wang, Nano Lett. **6**, 1656 (2006).
[4] Z. L. Wang and J. Song, Science **312**, 242 (2006).
[5] M. H. Huang, S. Mao, H. Feick, H. Yan, Y. Wu, H. Kind, E. Weber, R. Russo, and P. Yang, Science **292**, 1897 (2001).
[6] B. Wen, J. E. Sader, and J. J. Boland, Phys. Rev. Lett. **101**, 175502 (2008).
[7] C. Q. Chen, Y. Shi, Y. S. Zhang, J. Zhu, and Y. J. Yan, Phys. Rev. Lett. **96**, 075505 (2006).
[8] M. Riaz, O. Nur, M. Willander, and P. Klason, Appl. Phys. Lett. **92**, 103118 (2008).
[9] X. Wang, J. Song, J. Liu, and Z. L. Wang, Science **316**, 102 (2007).
[10] Z. L. Wang, Adv. Funct. Mater. **18**, 3553 (2008).
[11] M. Alexe, S. Senz, M. A. Schubert, D. Hesse, and U. Gösele, Adv. Mater. **20**, 4021 (2008).
[12] Y. Gao and Z. L. Wang, Nano Lett. **7**, 2499 (2007).
[13] J. Zhou, P. Fei, Y. Gu, W. Mai, Y. Gao, R. Yang, G. Bao, and Z. L. Wang, Nano Lett. **8**, 3973 (2008).

[14]J. Zhou, Y. Gu, P. Fei, W. Mai, Y. Gao, R. Yang, G. Bao, and Z. L. Wang, Nano Lett. **8**, 3035 (2008).
[15]H. J. Xiang, Y. Jinlong, J. G. Hou, and Z. Qingshi, Appl. Phys. Lett. **89**, 223111 (2006).
[16]Z. C. Tu and X. Hu, Phys. Rev. B **74**, 035434 (2006).
[17]A. Mitrushchenkov, R. Linguerri, and G. Chambaud, J. Phys. Chem. C **113**, 6883 (2009).
[18]A. J. Kulkarni, M. Zhou, and F. J. Ke, Nanotechnology **16**, 2749 (2005).
[19]L. Dai, W. C. D. Cheong, C. H. Sow, C. T. Lim, and V. B. C. Tan, Langmuir **26**, 1165 (2009).
[20]R. Agrawal, B. Peng, and H. D. Espinosa, Nano Lett. **9**, 4177 (2009).
[21]P. J. Michalski, N. Sai, and E. J. Mele, Phys. Rev. Lett. **95**, 116803 (2005).
[22]Z. Rong, W. Dingqu, X. Shaoqing, Z. Zhaoying, and Y. Xiongying, Nanotechnology **19**, 285712 (2008).
[23]M. L. Dunn and M. Taya, Proc. R. Soc. London, Ser. A **443**, 265 (1993).
[24]T. Brockmann and R. Lammering, Proc. Appl. Math. Mech. **1**, 139 (2002).
[25]H. Berger, S. Kari, U. Gabbert, R. Rodriguez-Ramos, J. Bravo-Castillero, R. Guinovart-Diaz, F. J. Sabina, and G. A. Maugin, Smart Mater. Struct. **15**, 451 (2006).
[26]F. Mohammadi, A. Khan, and R. B. Cass, "*Power Generation from Piezoelectric Lead Zirconate Titanate Fiber Composites*," MRS Symposia Proceedings No. 734 (Materials Research Society, Pittsburgh, 2003), p. D5.51.
[27]S. Xu, Y. Qin, C. Xu, Y. Wei, R. Yang, and Z. L. Wang, Nat. Nanotechnol. **5**, 366 (2010).
[28]H. L. Cox, Br. J. Appl. Phys. **3**, 72 (1952).
[29]X. L. Gao and K. Li, Int. J. Solids Struct. **42**, 1649 (2005).
[30]K. Momeni and R. S. Yassar, J. Comput. Theor. Nanosci. **6**, 1511 (2009).
[31]J. F. Nye, *Physical Properties of Crystals* (Oxford, London, 1957).
[32]W. D. Callister, *Materials Science and Engineering: An Introduction* (Wiley, New York, 2003).
[33]X. D. Bai, P. X. Gao, Z. L. Wang, and E. G. Wang, Appl. Phys. Lett. **82**, 4806 (2003).
[34]Y. Huang, X. Bai, and Y. Zhang, J. Phys.: Condens. Matter **18**, L179 (2006).
[35]H. Ni and X. Li, Nanotechnology **17**, 3591 (2006).
[36]M. P. Manoharan, A. V. Desai, G. Neely, and M. A. Haque, J. Nanomater. **2008**, 1 (2008).
[37]S. Hoffmann, F. Ostlund, J. Michler, H. J. Fan, M. Zacharias, S. H. Christiansen, and C. Ballif, Nanotechnology **18**, 205503 (2007).
[38]J. Song, X. Wang, E. Riedo, and Z. L. Wang, Nano Lett. **5**, 1954 (2005).
[39]G. Wang and X. Li, Appl. Phys. Lett. **91**, 231912 (2007).
[40]M. A. Schubert, S. Senz, M. Alexe, D. Hesse, and U. Gosele, Appl. Phys. Lett. **92**, 122904 (2008).
[41]N. Ashkenov, B. N. Mbenkum, C. Bundesmann, V. Riede, M. Lorenz, D. Spemann, E. M. Kaidashev, A. Kasic, M. Schubert, M. Grundmann, G. Wagner, H. Neumann, V. Darakchieva, H. Arwin, and B. Monemar, J. Appl. Phys. **93**, 126 (2003).
[42]G. Carlotti, G. Socino, A. Petri, and E. Verona, Appl. Phys. Lett. **51**, 1889 (1987).
[43]E. E. Gdoutos, *Fracture Mechanics Criteria and Applications* (Kluwer Academic, Dordrecht, 1990).
[44]M. Miwa, A. Takeno, K. Yamaguchi, and A. Watanabe, J. Mater. Sci. **30**, 2097 (1995).
[45]A. V. Desai and M. A. Haque, Appl. Phys. Lett. **91**, 183106 (2007).